Multi-objective Design Optimization of Square Tube with Circular Ring Filler Using RSM

*Muhammad Hafiz Aziz, Hafizan Hashim**
School of Mechanical Engineering, College of Engineering, Universiti Teknologi MARA, 40450, Shah Alam, Selangor
**hafizandes@gmail.com*

Hanita Hashim
Faculty of Engineering and Life Sciences, Science and Biotechnology Cluster, Universiti Selangor (UNISEL), Jln Timur Tambahan, 45600 Bestari Jaya, Selangor, Malaysia.

ABSTRACT

Square tubes with ring fillers are considered new form of tube energy absorbers that require further investigation. The aim of this work is twofold. Firstly, to develop the finite element (FE) model of the tubes. Secondly, to develop and optimize the response surface models of the specific energy absorption (SEA) and the crush force efficiency (CFE). The FE model of ring-filled square tube energy absorber subjected to three- point bending was developed using ABAQUS. A set of computational experiment was designed to investigate the effect of varying some factors on the SEA and CFE. Then, the response surface models of these two objectives were developed. Multi-objective optimization was performed to obtain the best factors' values for optimum objective values. Results showed that RSM managed to model the SEA and CFE. It is found that the optimal design of the ring-filled tube can be achieved if the thickness of the ring filler used is maximum, diameter at minimum, and medium in height.

Keywords: *Bending; Optimization; Energy Absorption; Finite Element Method*

eISSN 2773-5494

Received for review: 2022-04-21
Accepted for publication: 2022-11-09
Published: 2022-11-13

Introduction

Square tube is a typical thin-wall structure being used in many applications such as civil structures, automotive, and aerospace. With the ability to absorb plastic energy effectively, metallic thin-wall tubes are excellent for crashworthiness studies. Besides having sufficient strength and durability, metallic tubes are much lighter in terms of weight ratio. Therefore, metallic thin-walled structures are essential for automobile industries in order to reduce carbon print in particular.

Early theoretical bending collapse of thin-walled rectangular tube under pure bending was produced by Kecman [1]. Mathematical equations that represent the hinge moment and rotation angle which include the collapse mechanism were proposed. Later, Cimpoeru and Murray [2] conducted the same pure bending test but at larger deflection. They managed to validate the predicted model developed by Kecman. Other collapse mechanism of square tube was proposed by Wierzbicki et al. [3] with different approach. Applying the concept of super-folding element into bending mechanism, a column was axially loaded to imitate the initial bending collapse behaviour. The developed analytical models were validated using numerical calculations.

Multi-cell square tubes exhibit higher SEA than typical square tubes when subjected to bending. A study indicated that the bending resistance of embedded multi-cell tubes improves for about 70% compared to empty tubes [4]. Instead of using embedded method, wrapping of multi-cell tubes with composites could be an option when appropriate housing tubes are unavailable. The SEA of Al/CFRP hybrid multi-cell tubes increased by up to 41% compared to Al multi-cell tubes. Besides, partial CFRP wrapping of the Al/CFRP tubes has further increased the SEA by 11% [5].

Square and circular shapes are typically used to study the effect of section shape on SEA in bending and other performances. Study on contribution of different cross section shapes to its SEA is somewhat limited [6]. Tubes filled with cellular metal cores [7] and foam [8] are among solutions which considered promising for better bending resistance and energy absorption. It is acknowledged that wall thickness and filled ratio are significant factors that could affect the bending resistance and SEA.

Corrugated sandwich panels have been widely used in many structural applications. There are different shape of corrugated cores, such as tube-reinforced honeycomb [9] and triangular [10][11]. Energy absorbed by sandwich panels can be controlled by varying the geometry of the core. Nowadays, material for sandwich core has evolved and become diverse in order to fulfil current needs especially those involving cost, functionality, and the environment. Functionally graded lattice core is a type of porous media which could imitate the structural characteristic of biological organism. The mechanical properties of lattice are more-like isotropic in terms of simplicity,

randomness, and inhomogeneity, make it superior than typical Al foam [12][13].

Newly introduced advanced fillers often come with costs. Therefore, study on low-cost filler or cross section shape is still relevant and evolving. In the present work, a flat vertically arranged circular ring was proposed as reinforcing element for a typical square tube energy absorber subject to three-point bending. This ring is expected to provide additional plastic deformation to increase the SEA and CFE. FE model of the specimen and experimental setup was developed using ABAQUS. Coupon tensile test was conducted to obtain material properties for use in simulation. A systematic computational experiment was setup using DOE software, Minitab. Three factors were identified which are the thickness, diameter, and height of the circular ring filler. The face-centered central composite design (CCD) was utilized for the DOE and analysis of variance (ANOVA) was conducted to investigate the significance of every factor. Next, response surface models were developed of which SEA and CFE are the functions of the geometrical factors. Factorial study based on the DOE was performed to study the interaction effects, and based on the developed models, multi-objective optimization design was applied to obtain recommendation from Minitab for optimal configuration of the tube.

Methodology

Finite Element Modelling

Figure 1 shows the full model of a rectangular tube with circular ring filler. The square tube has side dimension of 50 mm and thickness of 1 mm. Length of the tube is 300 mm and the circular ring filler is placed vertically flat in the middle of the tube. The tube was modeled using robust conventional shell elements, S4R, which is a four-noded quadrilateral element with six degrees of freedom per node while the indenter and rigid support were modeled using R3D4 rigid element. S4R is suitable for large strain analyses with ability to enhance hourglass control. To allow nonlinear material behavior, five integration points was employed through the shell thickness. From detail observation of the preliminary simulation, the deformation mode of full and quarter model can be treated symmetrically. Therefore, quarter models were used to reduce the number of degrees of freedom (DOFs) and computational time as shown in Figure 3.

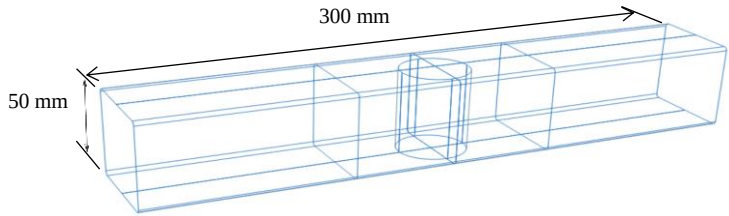

Figure 1: Full model of the filled square tube

Mesh Convergence Study

The most fundamental in constructing an accurate FE model are the correct element type and its required smallness. Figure 2 shows maximum indentation force versus element size in the refine mesh or hinge region. The crush load converged as the mesh density increased. Therefore, the element size of 2.0 x 2.0 mm is chosen to model the hinge region, while the rest of parts with a size of 5.0 x 2.0 mm.

The hinge region which is the middle part of the tube is separated by the partition line as seen in Figure 1. To avoid an infinite stress, a radius of 2 mm at every corner of the tube was introduced and based on the convergence study the radius size is reasonable as well as number of elements spaced around the corner area.

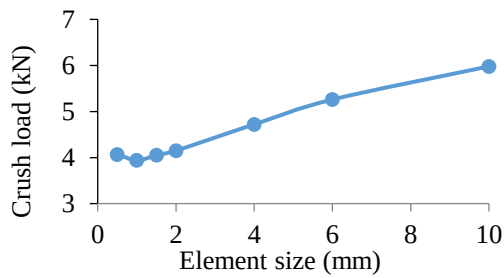

Figure 2: Mesh convergence of S4R element for the filled square tube

Loading, Interaction, and Boundary Condition

Figure 3 shows quarter FE model of the tube. The indenter moves downward along the y axis to produce a uniform centralized load. A fully constrained rigid cylinder is used as the support and it is located 50 mm from edge. Reference node is tagged to both indenter and support to ease motion control as a whole body.

Boundary conditions along longitudinal axis (i.e. z axis) are applied constraining x displacement and rotation y and z. The cross-sectional area is constrained by z displacement and rotation x and y. Step time used in this analysis is 0.03 s which is the value from frequency linear perturbation analysis. Under amplitude option, smooth step is selected for a smooth indentation throughout the total step time. All contact surfaces in the present FE model are treated with 0.25 friction coefficient except those contacted with rigid surfaces which are frictionless.

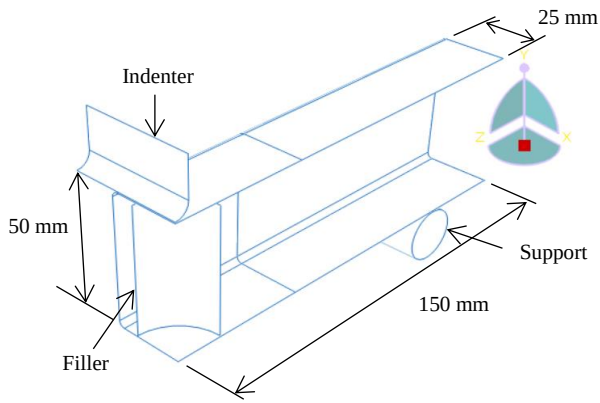

Figure 3: Computational experimental setup of three-point bending

Material Model

The tube was modeled with a piecewise linear elastic-plastic material model with strain hardening. Coupon tensile test was conducted using the Instron model 3382 Universal Testing Machine (UTM). The material properties for the aluminium are as follows: initial yields stress; σ_y=173 MPa, Young's modulus; E=60 GPa, Poisson ratio; $\nu = 0.33$, Ultimate Tensile Strength (UTS); σ_u=220 MPa, and density; ρ=2700 kg/m^3. The engineering stress-strain curve of the material was obtained using a standard tensile test in accordance with AS1391-1991(1991). Figure 4 shows the true stress-strain curve from coupon tensile test. The ancillary strain data was converted into true strain by using,

$$\varepsilon_{true} = \ln(1 + \varepsilon) \tag{1}$$

where, $\varepsilon =$ experimental strain. The true stress data was converted using,

$$\sigma_{true} = \sigma \cdot (1 + \varepsilon) \tag{2}$$

where, $\sigma =$ experimental stress.

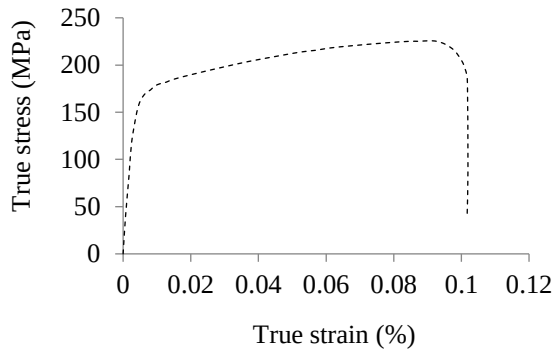

Figure 4: True stress-strain curve from tensile test for Al 6063-T5.

Response Surface Models

A DOE was created based on a two level Central Composite Design (CCD) with full factorial. Table 1 shows the independent variables and design levels used. Minitab had been used starting from DOE, analysis of response surface, and optimization. Table 2 tabulates different combination of design variables with corresponding design responses. The FE model used in this experiment are subjected to quasi-static loading, in order for the specimen to absorb as much as possible the crush energy.

SEA is defined as the energy absorbed per unit mass of material as shown in (3). The higher the value of SEA, the higher the amount of energy absorbed and the lighter the energy absorber would be. The CFE is another crashworthiness indices used to evaluate the consistency of collapse load. It is defined as the ratio of mean load to initial peak load as shown in (4). The best absorber will have a crush force efficiency of 100% or ratio one, which is hard to achieve.

$$\text{SEA} = \text{Energy absorbed/Mass} \quad (3)$$

$$\text{CFE} = (\text{Mean Load/Initial Peak Load}) \times 100\% \quad (4)$$

Table 1: Independent variables and two levels of experiment

Variables (mm)	Code	-1	1
Thickness	T	1	2
Diameter	D	40	48
Height	H	40	48

Table 2: The design matrix

Run Order	Blocks	T (mm)	D (mm)	H (mm)	SEA (kJ/kg)	CFE
1	1	1	40	40	1.5866	0.7942
2	1	2	40	40	1.8458	0.8409
3	1	1	48	40	1.5136	0.8333
4	1	2	48	40	1.7325	0.8603
5	1	1	40	48	1.7967	0.7116
6	1	2	40	48	2.2660	0.7304
7	1	1	48	48	1.7237	0.6596
8	1	2	48	48	2.2937	0.7114
9	1	1	44	44	1.5979	0.7398
10	1	2	44	44	1.9829	0.7366
11	1	1.5	40	44	1.9200	0.8066
12	1	1.5	48	44	1.7363	0.8237
13	1	1.5	44	40	1.6394	0.8186
14	1	1.5	44	48	1.9452	0.6896
15	1	1.5	44	44	1.7615	0.7307

Results

A second order model was utilised, and regression analysis using the least square approach was performed to obtain the polynomial coefficients of the empirical functions between the two responses and three input parameters. The regression equations for SEA and CFE are shown in (3) and (4) respectively.

SEA = 11.74 - 1.446 T - 0.326 D - 0.123 H + 0.039 T*T + 0.00297 D*D + 0.00073 H*H
+ 0.00378 T*D + 0.03506 T*H + 0.001102 D*H (3)

CFE = 3.87 + 0.327 T - 0.2295 D + 0.0918 H - 0.1092 T*T + 0.003102 D*D - 0.000716 H*H + 0.00084 T*D - 0.00019 T*H - 0.001014 D*H (4)

ANOVA

A statistical metric called R^2 is used to verify the viability of a regression model that fits real data points [14]. The higher the R^2 number, the better the match between the observational model and the real data. Besides, F-value evaluate the ratio of the regression mean square to the remaining mean square. The F-value has a critical value that represent as F_0, and the P-value represents the chance of $F < F_0$ [15]. Table 3 show the ANOVA for SEA. Result shows that the model is significant as well as the three input parameters involved. The value of R^2 is 98.64% that indicates a good fit at high accuracy and this leads to improved fitness nature.

Table 3: ANOVA for SEA

Source	DF	Adj SS	Adj MS	F-Value	P-Value
Model	9	0.724241	0.080471	40.42	0.000
Linear	3	0.670631	0.223544	112.28	0.000
T	1	0.361913	0.361913	181.78	0.000
D	1	0.017231	0.017231	8.65	0.032
H	1	0.291487	0.291487	146.40	0.000
Square	3	0.011329	0.003776	1.90	0.248
T*T	1	0.000245	0.000245	0.12	0.740
D*D	1	0.005806	0.005806	2.92	0.148
H*H	1	0.000353	0.000353	0.18	0.691
2-Way Interaction	3	0.042281	0.014094	7.08	0.030
T*D	1	0.000456	0.000456	0.23	0.652
T*H	1	0.039340	0.039340	19.76	0.007
D*H	1	0.002485	0.002485	1.25	0.315
Error	5	0.009955	0.001991		
Total	14	0.734196			
R^2				98.64%	

Table 4 shows ANOVA for the CFE of the tube. Two factors in linear interaction (i.e. T and D) seems non-significant and the value of R^2 is 95.95%, slightly lower than of the SEA. For a cleaner result, non-significant input variables can be excluded from interaction list to make way for the second test

block in order to simplify the model. However, in this work, the non-significant factors are left in the regression equation to show the parameter estimate.

Table 4: ANOVA for CFE

Source	DF	Adj SS	Adj MS	F-Value	P-Value
Model	9	0.052520	0.005836	13.15	0.006
Linear	3	0.043557	0.014519	32.71	0.001
T	1	0.001995	0.001995	4.49	0.088
D	1	0.000002	0.000002	0.01	0.946
H	1	0.041560	0.041560	93.63	0.000
Square	3	0.006840	0.002280	5.14	0.055
T*T	1	0.001919	0.001919	4.32	0.092
D*d	1	0.006336	0.006336	14.27	0.013
H*H	1	0.000337	0.000337	0.76`	0.423
2-Way Interaction	3	0.002123	0.000708	1.59	0.301
T*D	1	0.000022	0.000022	0.05	0.831
T*H	1	0.000001	0.000001	0.00	0.960
D*H	1	0.002099	0.002099	4.73	0.081
Error	5	0.002219	0.000444		
Total	14	0.054740			
R^2				95.95%	

Interaction and Main Effects of Input Variables

Figure 5 shows the interaction plots for SEA and CFE of the tube. It can be seen that when diameter size increases from 40 to 44 mm, the SEA and CFE are both deteriorate. This may be attributed to additional material in the filler that leads to extra mass and higher flexural strength. Further increasing of diameter size shows non-significant improvement in SEA and CFE. The SEA increases significantly when thickness and height of the ring increase. This is due to the extra material and stroke that provides more and lengthy stroke for plastic. This however does not apply to CFE since further increase of these two factors has worsened the situation because CFE is inversely related to the peak load of force versus deflection graph. Higher value of thickness and height of the ring filler produces larger peaks which reduce the CFE while smaller peaks increase the CFE to its maximum value of 1 (one). Same finding was reported in [16] when better CFE index was achieved by tubes with smaller mass or lesser material. Moreover, it is also observed that diameter of circular ring filler affects SEA and CFE the least among all the three input variables.

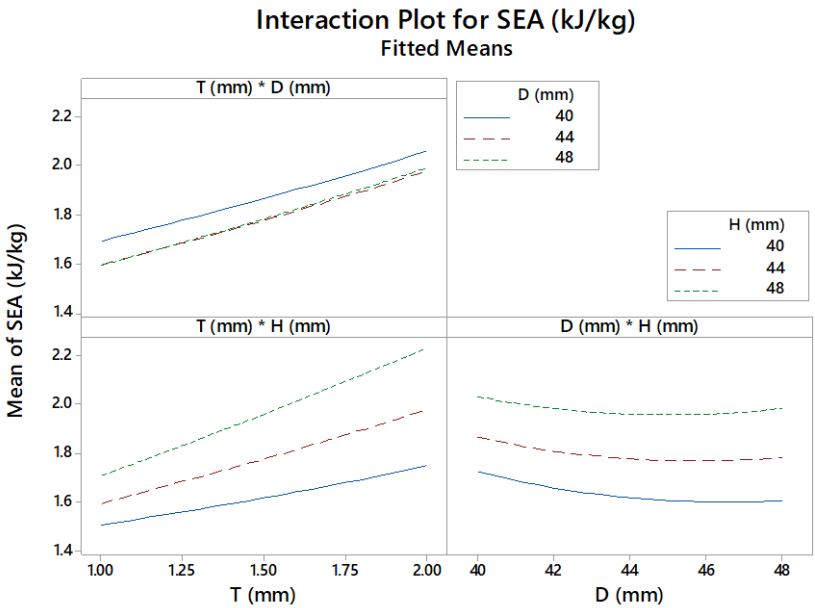

(a)

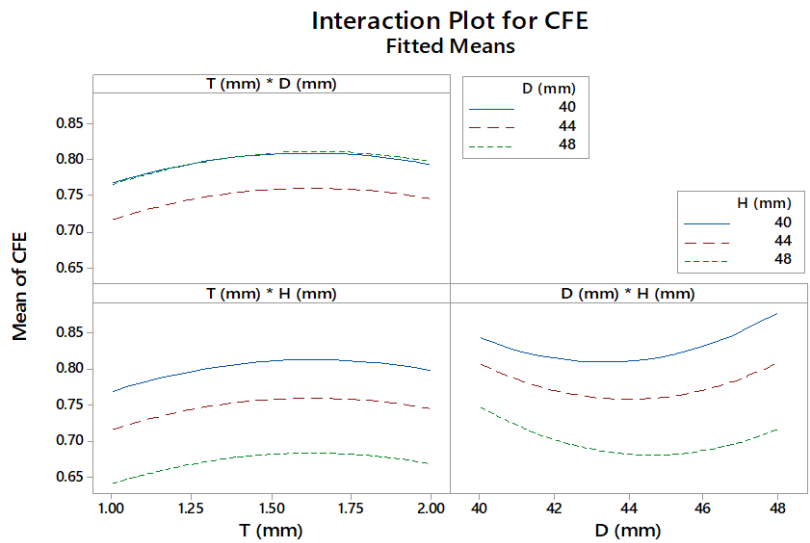

(b)

Figure 5: Interaction plot for (a) SEA and (b) CFE of the ring-filled square tube

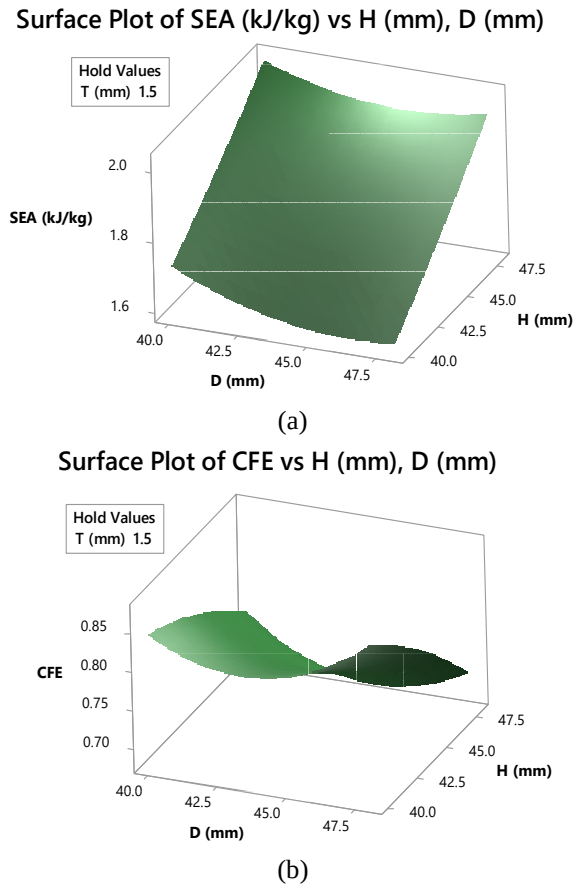

Figure 6: Surface plot for (a) SEA and (b) CFE of the ring-filled square tube

Figure 6 illustrates the response surface plot for SEA and CFE of the ring-filled tube respectively with respect to ring's height and diameter. It can be seen that a greater amount of SEA can be absorbed if smaller diameter and longer circular ring filler were used. For the CFE, the interaction was opposite where shorter filler with larger diameter were required for greater absorption.

Optimization

Figure 7 shows the optimization plot that indicates variables setting that optimize the SEA and CFE. Maximum thickness is preferable because it produces higher SEA that is closer to the target of 2.0831 kJ/kg. However, for higher CFE, desired thickness is approximately 2/3 of the max thickness.

Instead, increasing the size of diameter is not desirable because it reduces SEA and CFE as a whole. However, CFE responses reversibly because at the max diameter it moves closer to the target of 0.7873. Increasing the height of the ring, increases the SEA and decreases the CFE. The bounds really affect the desirability values in CFE and composite because the predicted responses are lower than the target.

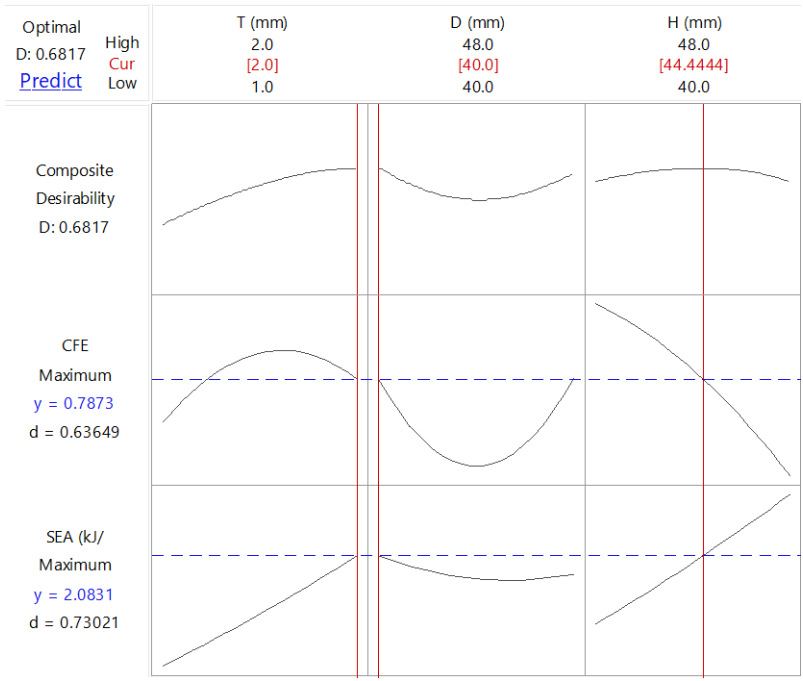

Figure 7: Dual optimum responses

Table *5:* Validation and repeatability test

Recommended parameter			Minitab	ABAQUS	Error (%)
	Max SEA	Max CFE			
T (mm)	2.0				
D (mm)	40.0				
H (mm)	44.4444				
SEA (kJ/kg)	2.0831		2.0831	1.9600	6.29
CFE		0.7302	0.7302	0.7871	7.23

Table 5 shows repeatability and validation test for the SEA and CFE under optimal conditions. From the validation tests, it can be seen that the difference errors are very small which shows a good agreement between the developed RSM models and the FE models. Therefore, the RSM based regression models can be used for predicting the SEA and CFE of the filled-circular tube with good accuracy.

Conclusion

In this work, the influence of thickness, diameter, and height of circular ring filler on the SEA and CFE performance of a square tube under three-point bending has been investigated. SEA and CFE were then being optimized using simulation-optimization RSM. A DOE based on face-centered CCD was used to develop an appropriate model using least-squares method. The regression models were tested and validated via ABAQUS. The percentage of errors obtained for both performances were less than ten percent. Multi objective optimization was performed and the optimal conditions were obtained at the T_{max}, D_{min}, and H_{med}.

References

[1] D. Kecman, "Bending collapse of rectangular and square section tubes," *Int. J. Mech. Sci.*, vol. 25, no. 9–10, 1983, doi: 10.1016/0020-7403(83)90072-3.

[2] S. J. Cimpoeru and N. W. Murray, "The large-deflection pure bending properties of a square thin-walled tube," *Int. J. Mech. Sci.*, vol. 35, no. 3–4, 1993, doi: 10.1016/0020-7403(93)90079-A.

[3] T. Wierzbicki, L. Recke, W. Abramowicz, and T. Gholami, "Stress profiles in thin-walled prismatic columns subjected to crush loading-I. Compression," *Comput. Struct.*, vol. 51, no. 6, 1994, doi: 10.1016/S0045-7949(05)80001-X.

[4] X. Zhang, H. Zhang, and K. Leng, "Experimental and numerical investigation on bending collapse of embedded multi-cell tubes," *Thin-Walled Struct.*, vol. 127, 2018, doi: 10.1016/j.tws.2018.03.011.

[5] Z. Huang and X. Zhang, "Crashworthiness and optimization design of quadruple-cell Aluminum/CFRP hybrid tubes under transverse bending," *Compos. Struct.*, vol. 235, 2020, doi: 10.1016/j.compstruct.2019.111753.

[6] D. Bilston, D. Ruan, A. Candido, and Y. Durandet, "Parametric study of the cross-section shape of aluminium tubes in dynamic three-point bending," *Thin-Walled Struct.*, vol. 136, 2019, doi:

10.1016/j.tws.2018.12.032.

[7] M. Vesenjak, I. Duarte, J. Baumeister, H. Göhler, L. Krstulović-Opara, and Z. Ren, "Bending performance evaluation of aluminium alloy tubes filled with different cellular metal cores," *Compos. Struct.*, vol. 234, 2020, doi: 10.1016/j.compstruct.2019.111748.

[8] B. Zhang, J. Zhang, L. Wang, Y. Jiang, W. Wang, and G. Wu, "Bending behavior of cenosphere aluminum matrix syntactic foam-filled circular tubes," *Eng. Struct.*, vol. 243, 2021, doi: 10.1016/j.engstruct.2021.112650.

[9] Y. Zhang, L. Yan, W. Zhang, P. Su, B. Han, and S. Guo, "Metallic tube-reinforced aluminum honeycombs: Compressive and bending performances," *Compos. Part B Eng.*, vol. 171, 2019, doi: 10.1016/j.compositesb.2019.04.044.

[10] F. Xia, T. X. Yu, Y. Durandet, and D. Ruan, "Triangular corrugated sandwich panels under longitudinal bending," *Thin-Walled Struct.*, vol. 169, 2021, doi: 10.1016/j.tws.2021.108359.

[11] I. Ali, S. Qi, P. Shi, M. Ammar, and A. Ali, "Investigation of mass distribution between core and face sheet on bending energy absorption of self-reinforced PP sandwich beams," *Thin-Walled Struct.*, vol. 159, 2021, doi: 10.1016/j.tws.2020.107283.

[12] Y. Nian, S. Wan, P. Zhou, X. Wang, R. Santiago, and M. Li, "Energy absorption characteristics of functionally graded polymer-based lattice structures filled aluminum tubes under transverse impact loading," *Mater. Des.*, vol. 209, 2021, doi: 10.1016/j.matdes.2021.110011.

[13] H. Yin, D. Guo, G. Wen, and Z. Wu, "On bending crashworthiness of smooth-shell lattice-filled structures," *Thin-Walled Struct.*, vol. 171, 2022, doi: 10.1016/j.tws.2021.108800.

[14] W. Xie *et al.*, "Process parameter optimization for thin-walled tube push-bending using response surface methodology," *The International Journal of Advanced Manufacturing Technology*, vol. 118, no. 11, pp. 3833–3847, Oct. 2021, doi: 10.1007/S00170-021-08196-8.

[15] S. Chamoli, "ANN and RSM approach for modeling and optimization of designing parameters for a v down perforated baffle roughened rectangular channel," *Alexandria Eng. J.*, vol. 54, no. 3, pp. 429–446, 2015, doi: 10.1016/j.aej.2015.03.018.

[16] H. Zhang and X. Zhang, "Crashworthiness performance of conical tubes with nonlinear thickness distribution," *Thin-Walled Struct.*, vol. 99, 2016, doi: 10.1016/j.tws.2015.11.007.